Intrinsic fluence non-uniformity in D3He backlit proton radiography

PSFC/JA-24-68

Intrinsic fluence non-uniformity in D^3He backlit proton radiography

T. M. Johnson,[1] J. Shan,[1] R. Kishimori,[1] M. J. Cufari,[1] P. J. Adrian,[1, 2] B. Buschmann,[1] C. W. Chang,[1] S. G. Dannhoff,[1] A. DeVault,[1] T. E. Evans,[1] B. Foo,[1] J. H. Kunimune,[1] Y. Lawrence,[1] J. A. Pearcy,[1] B. L. Reichelt,[1] L. Russell,[1] G. D. Sutcliffe,[1, 3] N. L. Vanderloo,[1] J. Vargas,[1] C. Wink,[1] M. Gatu Johnson,[1] F. H. Séguin,[1] R. D. Petrasso,[1] J. A. Frenje,[1] and C. K. Li[1]

[1]*Massachusetts Institute of Technology, Cambridge, Massachusetts 02139, USA*
[2]*Los Alamos National Laboratory, Los Alamos, New Mexico 87545, USA*
[3]*Lawrence Livermore National Laboratory, Livermore, California 94550, USA*

April 2024

Plasma Science and Fusion Center
Massachusetts Institute of Technology
Cambridge MA 02139 USA

This work was supported in part by the U.S. Department of Energy NNSA MIT Center-of-Excellence under Contract DE-NA0003868 and by the National Laser Users Facility under Contract No. DE-NA0003938. Reproduction, translation, publication, use and disposal, in whole or in part, by or for the United States government is permitted.

Submitted to *Review of Scientific Instruments*

Intrinsic fluence non-uniformity in D^3He backlit proton radiography

T. M. Johnson,[1, a)] J. Shan,[1] R. Kishimori,[1] M. J. Cufari,[1] P. J. Adrian,[1, 2] B. Buschmann,[1] C. W. Chang,[1] S. G. Dannhoff,[1] A. DeVault,[1] T. E. Evans,[1] B. Foo,[1] J. H. Kunimune,[1] Y. Lawrence,[1] J. A. Pearcy,[1] B. L. Reichelt,[1] L. Russell,[1] G. D. Sutcliffe,[1, 3] N. L. Vanderloo,[1] J. Vargas,[1] C. Wink,[1] M. Gatu Johnson,[1] F. H. Séguin,[1] R. D. Petrasso,[1] J. A. Frenje,[1] and C. K. Li[1]

[1)]*Massachusetts Institute of Technology, Cambridge, Massachusetts 02139, USA*
[2)]*Los Alamos National Laboratory, Los Alamos, New Mexico 87545, USA*
[3)]*Lawrence Livermore National Laboratory, Livermore, California 94550, USA*

(Dated: 2 August 2024)

Proton radiography is an essential diagnostic for studying magnetic fields in high energy density physics experiments. Protons are born in a fusion implosion, traverse the plasma, and are detected on CR-39 solid state nuclear track detectors. Here, it is shown that there is an intrinsic non-uniformity in ~ 15 MeV D^3He proton radiography data. The increasing angle between the proton trajectory and the center of the detector results in the proton traveling through more detector stack material. As the protons travel through more material and lose energy, the proton energy spectrum gets wider. Protons at the lower end of the spectrum can therefore be lost. The nominal filtering results in protons being ranged out at large angle, causing the intrinsic non-uniformity. This angular effect is confirmed with both OMEGA experiments and Geant4 simulations. It is found that reducing the filtering between the pieces of CR-39 in the detector stack mitigates this effect. Results from accelerator experiments show that this reduced filtering does not impact the detection efficiency of the CR-39. Accounting for this intrinsic fluence non-uniformity is essential for magnetic field reconstruction techniques using proton radiographs.

I. INTRODUCTION

Proton radiography is a vital diagnostic for high energy density physics experiments. It is one of very few diagnostics that is able to measure magnetic fields in high energy density laser driven plasmas. Proton radiography has been used to measure the strength of Biermann-battery generated fields, explore the physics of magnetic reconnection, and show the amplification of magnetic fields through a turbulent dynamo[1–5]. Recent advances in the field have allowed for the numerical reconstruction of magnetic and electric fields responsible for recorded radiographs[6–8].

A typical proton radiography experiment uses a proton source to generate MeV-scale energy protons to probe an experimental plasma[9–11]. As the protons traverse the plasma, they are deflected by the electromagnetic fields inside the plasma. This results in a slight bend in the proton trajectory once it leaves the plasma. After some distance, the protons are recorded on a detector. The resulting radiograph is a 2D histogram of the proton hits on the detector.

Numerical reconstruction techniques typically require knowledge of the radiograph fluence in the absence of the plasma[6,7]. This is often assumed to be a uniform flat field fluence. Several experiments have been impacted by non-uniform backgrounds[12]. There are several possible explanations for the non-uniformity, such as capsule charging and electromagnetic fields in the implosion corona[13]. Here, it is shown that there is an intrinsic particle ranging effect that results in a non-uniform radiograph in the absence of the plasma for D^3He proton radiography. The non-negligible angle of the proton with respect to the detector near the edges of the radiograph results in more energy loss as the protons travel through the filtering. The end result is that fewer protons are detected with increasing angles causing the non-uniformity.

This paper is organized in the following manner: Section II explains the physical origin of the non-uniformity in detail and shows experimental evidence of the effect; Section III details the results of Geant4 Monte-Carlo simulations which show that reducing the thickness of filters in the detector stack can mitigate the non-uniformity; Section IV reports on accelerator experiments confirming that reducing the filtering does not reduce the detection efficiency; and Section V concludes the paper.

II. ORIGIN OF THE FLUENCE NON-UNIFORMITY

Protons for proton radiography can be generated either through target normal sheath acceleration or a backlighter capsule fusion implosion[9–11]. At the OMEGA laser facility, there are enough laser beams available to implode a capsule to generate fusion protons while simultaneously driving a physics experiment[14]. The typical geometry of an OMEGA proton radiography experiment is shown in Figure 1 A). The capsule is filled with an equimolar mixture of deuterium and helium-3 to provide high energy protons through the DD and D^3He fusion reactions, which produce 3 MeV and 14.7 MeV protons, respectively. Since the laser is typically still on when the protons are born in the implosion, their energies are upshifted[12,15]. For this reason, D^3He protons in this configuration typically have a mean energy of about 15 MeV. Backlit proton radiography uses CR-39 as a detector[16].

A filter stack is required to downrange the protons into the detectable energy range of the CR-39. The specifics of the CR-39 detectable energy range are complicated and inherently depend on the microscope scanning system settings[16]. Protons break molecular bonds in the CR-39. Etching the CR-39

[a)]tmarkj@mit.edu

in an 6 molar NaOH eats away at the regions where the molecular bonds are broken to reveal particle tracks. The amount of energy deposited by the protons is directly related to the size of the particle tracks. Due to the shape of the stopping power curve of protons in CR-39 above the Bragg peak, high energy protons deposit relatively less energy and have smaller tracks while lower energy protons deposit a larger amount of energy and have large tracks. Between proton energies of around .5 MeV to about 4 MeV, CR-39 has 100% detection efficiency[16]. Energies lower than this do not deposit much energy and therefore are difficult to detect. The shape of the higher energy part of the CR-39 detection efficiency curve depends on the etch time and the microscope contrast limits[16]. Etching CR-39 for longer increases the size of all tracks and helps the high energy tracks become visible. CR-39 is typically etched as long as possible before the tracks begin to overlap[17]. The proton fluence from the backlighter is typically high enough to limit the etch time to between 1.5 and 3 hours for D^3He protons with 5 hours being the maximum etch time typically used[18]. To eliminate intrinsic CR-39 noise, it is often necessary to remove high-contrast fainter tracks[16]. Since high energy tracks are typically higher-contrast since they do not break as many molecular bonds, removing noise can also remove real proton tracks, reducing the detection efficiency.

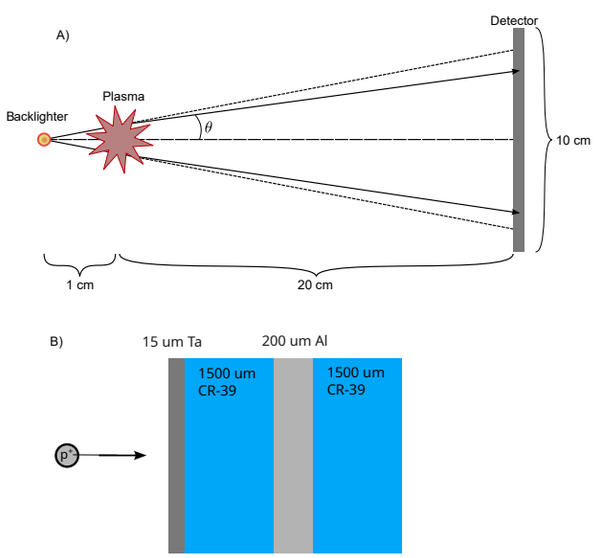

FIG. 1. A) Diagram of a standard proton radiography experimental setup. Protons are created inside the fusion implosion and travel to the experimental subject plasma where they are deflected. After leaving the plasma, the protons travel through the vacuum until they reach the detector stack. The angle θ is defined as the angle between the proton trajectory and the center of the detector. B) Details of the proton radiography detector stack. There are four layers in the detector stack: 15 μm Ta, 1500 μm CR-39, 200 μm Al, and 1500 μm CR-39.

The filter stack, shown in Figure 1 B), is composed of four layers to accomplish several important tasks. The first layer is a thin tantalum foil which blocks out any low energy ablator ions from the implosion[19]. It is typically 15 μm thick to avoid ranging out the lower energy DD protons. The second layer is the first piece of CR-39 which detects the DD fusion protons. The $\sim$ 15 MeV D^3He protons are too high energy at this stage to be detected by the first CR-39 detector. Even after the D^3He protons exit the first CR-39 detector, they are still too high energy to be detected. The third layer is an aluminum filter which acts to slow down the D^3He protons into the detectable energy range of CR-39. This aluminum filter is typically 100 to 200 μm thick with the actual thickness used in an experiment depending on the thickness of the first piece of CR-39. The last part of the detector stack is a second CR-39 detector used to detect the downranged D^3He protons. The first three layers of the detector stack serve as the filtering for the D^3He protons.

The protons are born in a small volume of around 50 μm diameter[1]. Typically, the proton backlighter is located 1 cm away from the subject plasma while the detector sits between 15 cm and 25 cm away from the plasma. This gives the system high magnification as shown in Figure 1 A). A result of the location of the detector is that protons at the edge of the detector have a non-zero angle with respect to the center of the detector. This causes the protons at larger angles to travel more distance through the detector stack which slows them down more. For the D^3He proton at 15 MeV, the longer path length can result in part of the spectrum falling below the lower bound of the CR-39 detectable energy range. The result of this is less protons being detected with increasing angle when compared to the true fluence on the detector. Figure 2 shows example spectra of D^3He protons at different angles. Note that the 3 MeV DD protons do not lose enough energy to be impacted by this effect.

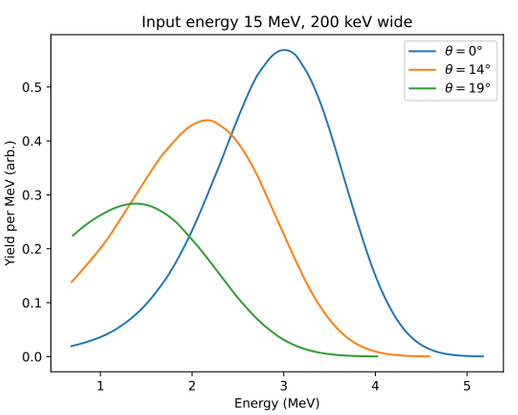

FIG. 2. Example D^3He proton spectra after traveling through the detector stack at different angles. For protons at the center of the detector, very few are below the detectable energy range of the CR-39. At larger angles of 14 degrees and 19 degrees, which respectively represent the edges and corners of the detector, more protons are below the detectable range of the CR-39. These spectra were generated using SRIM stopping power tables to range protons through a detector stack of 15 μm Ta, 1500 μm CR-39, and 150 μm Al[20]. The input D^3He proton spectrum had a mean energy of 15.0 MeV and a standard deviation of 200 keV[10].

This angle effect can be described mathematically through the following equation:

$$\Phi(\theta) = \Phi_0 \cos(\theta) \int_0^\infty \frac{dN}{dE}(E,\theta) f(E,\theta) dE, \qquad (1)$$

where θ is the angle of the proton with respect to the normal vector of the detector, Φ_0 is the base fluence at the center of the detector, dN/dE is the proton energy spectrum on the CR-39 which depends on both energy and angle, and $f(E,\theta)$ is the detection efficiency of the CR-39. The $\cos(\theta)$ term is a solid angle term which accounts for the edges of the detector being physically farther away from the implosion compared to the center. The integral in the equation serves to count the number of protons that make it into the detectable energy range of the CR-39. The detection efficiency of the CR-39 is often assumed to be a box car function with 100% detectablity between 0.5 MeV and 4 MeV. While large angles can reduce the detection efficiency of the CR-39, angles below 20 degrees show minimal reduction[21]. Using both of these assumptions, equation 1 can be simplified to the following expression:

$$\Phi(\theta) = \Phi_0 \cos(\theta) \int_{0.5\text{ MeV}}^{4\text{ MeV}} \frac{dN}{dE}(E) dE. \qquad (2)$$

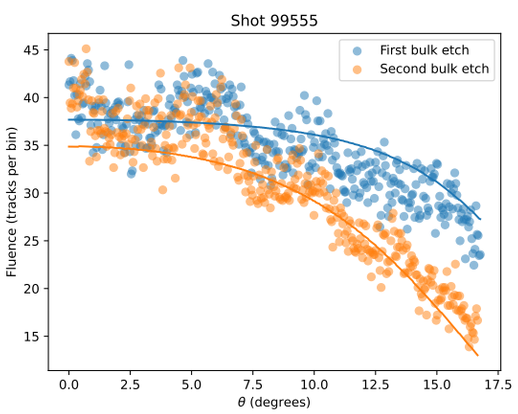

FIG. 3. Comparison between the angular fluence profile from D^3He proton radiographs collected at OMEGA. The bin size is 18.17 μm by 18.17 μm. The blue points correspond to the D^3He proton radiograph using the standard detector stack and 110 μm of CR-39 via bulk etching, a technique that evenly removes material from the CR-39 surface. The orange points correspond to the D^3He proton radiograph after 160 μm of CR-39 is removed from the detector (a difference of 50 μm between the blue and orange points). There is originally some reduction in the fluence at large angle but the additional thickness of CR-39 increases this effect. The solid lines correspond to equation 2 with the proton spectrometer measurements for the proton spectrum.

Experimental evidence of the angular profile in D^3He proton radiographs was collected on a proton radiography experiment at OMEGA. The data were taken on a null shot where the main physics experiment did not happen. The result was a blank radiograph showing no detailed structures. Figure 3 shows the resulting angular profile of the D^3He proton radiograph. With track etching, the radiation damaged regions etch faster than the undamaged regions[22]. Bulk etching removes material from both the damaged and undamaged regions at the same rate and is used to remove bulk material from the surface of the CR-39. Since the radiograph was underfiltered, both angular profiles shown in Figure 3 were bulk etched. The data in blue was bulk etched to 110 μm while the data in orange was bulk etched for an additional 50 μm for a total bulk etch of 160 μm. Therefore, the second bulk etch profile shows the proton fluence after the protons have traveled through this additional 50 um of CR-39. Wedge range filter (WRF) proton spectrometers[16] were fielded on the laser shot and measured a D^3He proton mean energy of 15.12 ± 0.06 MeV and a width of $.21 \pm 0.01$ MeV. The WRF results were used with equation 2 using SRIM stopping power tables to generate the solid curves in Figure 3. The model captures the main features of the data and shows that more proton energy loss results in a reduction of the fluence at large angles.

III. GEANT4 MODELING

The Monte-Carlo code Geant4 was used to model the passage of D^3He protons through the detector stack[23–25]. Geant4 considers energy straggling which is a physical phenomenon where high energy charged particles undergo small angle scattering events which makes them deviate from a completely straight trajectory. A scattered particle travels more distance before exiting the material which results in more energy loss. The `emstandardSS` Geant4 physics list was used because it considers energy straggling. The Geant4 model has the same geometry as shown in Figure 1 but without a subject plasma. The protons are generated at a single point and propagate isotropically into 4π. The simulated detector stack was the same as described previously.

The Geant4 simulation was used to study how the thickness of the Al filtering impacts the fluence non-uniformity. Figure 4 shows the results of this comparison. Protons were generated at realistic fluence levels and a lineout was taken from the center of the detector to the corner. This was repeated for different thicknesses of alumimum filtering. The results show that for 175 μm and 200 μm of Al, the profile is quite severe. For 150 μm of Al, the profile is considerably reduced and is almost the same as the solid angle profile. For the detector stack with 1500 μm CR-39, the normal filtering is 175 μm or 200 μm Al. The Geant4 simulations suggest that reducing this filtering to 150 μm Al would largely mitigate the profile non-uniformity.

The issue with reducing the thickness of the filtering is that higher energy protons near the center could exceed the detectable energy range for protons in CR-39. As discussed previously, the high energy cutoff of the CR-39 detectable energy range is not well known. Experiments are needed to demonstrate that using less filtering does not reduce the detection efficiency of D^3He protons.

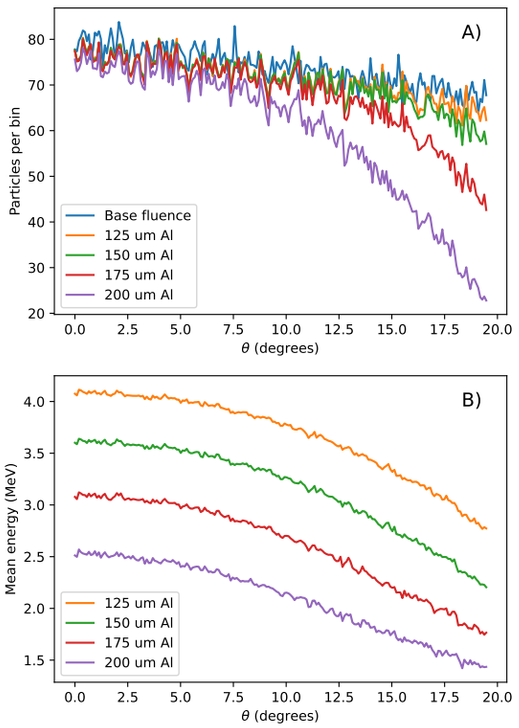

FIG. 4. A) Resulting profiles from the Geant4 simulations with different thicknesses of aluminum filtering. With 200 μm and 175 μm of Al, the fluence is greatly reduced with increasing angle. With 150 μm of Al, the fluence profile is almost the same as the base fluence. B) Mean energy of the protons as a function of angle for the different thicknesses of aluminum. For all thicknesses, the mean energy decreases as a function of angle as expected.

IV. ACCELERATOR MEASUREMENTS OF CR-39 EFFICIENCY

In order to confirm that reducing the filtering would not result in a reduction in the CR-39 detection efficiency, accelerator experiments were carried out. A 125 kV electrostatic ion accelerator was used to accelerate deuterium ions and collide them with a ^{3}He doped ErD_2 target to produce D^{3}He fusion protons[26]. The CR-39 detection efficiency was measured for different filtering using a surface barrier detector (SBD) and CR-39 co-holder[27]. This co-holder enables an absolute measurement of the proton fluence and proton spectrum incident on the CR-39 using the SBD. A schematic of the accelerator experimental setup is shown in Figure 5. A 15 μm thick Ta overlay filter covers the detector stack. The proton spectrum behind this filter had a mean energy of 14.21 ± 0.05 MeV and a width of 109 ± 2 keV as measured by the SBD. Since the energy of the protons going into the detector stack is slightly different from real proton radiography experiments, the detector stack was modified. The new stack had 15 μm Ta, 1500 μm CR39, and either 75 μm or 125 μm Al.

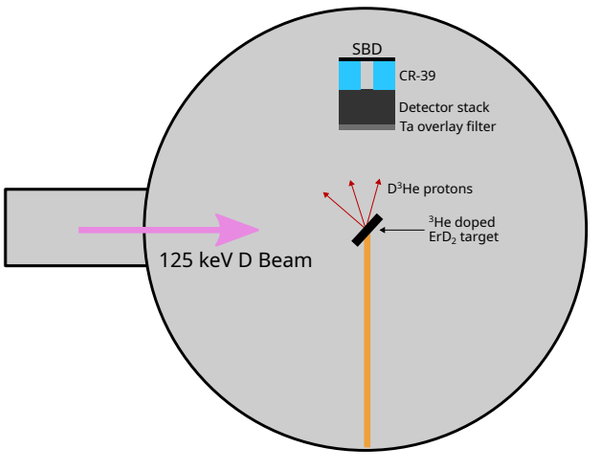

FIG. 5. Schematic of the accelerator experiment. A deuterium beam at 125 keV collides with a ^{3}He doped ErD_2 target to produce D^{3}He protons. These protons first travel through a 15 μm thick Ta overlay filter after which they travel through the detector stack. Behind the detector stack, protons are detected on both a piece of CR-39 and the SBD. The CR-39 has a hole in the center which allows the CR-39 and SBD to see the same proton spectrum.

Table I summarizes the results from the accelerator experiment. For both thicknesses of aluminum, the detection efficiency is very close to 100% for an etch time of 5 hours. The mean energies for both of these configurations, as shown in the Table I, are comparable to the Geant4 simulations with 125 μm and 200 μm Al. This shows that reducing the thickness of the Al filtering can eliminate the fluence non-uniformity while still having near 100% detection efficiency.

TABLE I. Results from the accelerator experiments. For both sets of filtering, the CR-39 detection efficiency is near 100%. The mean energy of the thinner case corresponds most closely to the 125 μm Al case. These results show that decreasing the filtering does not reduce the detection efficiency of the CR-39.

	CR-39 efficiency	Mean energy (MeV)	Width (keV)
Thinner Al	0.986 ± 0.020	4.27 ± 0.05	399 ± 6
Thicker Al	0.957 ± 0.020	2.71 ± 0.05	523 ± 6

V. CONCLUSION

The relatively close distance between the proton backlighter and the CR-39 detector can result in a non-uniform fluence profile in proton radiography experiments. Protons at the corners and edges of the detector pass through appreciably more material than protons at the center. This results in more energy loss for the protons farther from the cen-

ter. The additional energy loss results in some protons being completely ranged out. Only D^3He protons are affected by this phenomenon since the DD protons do not experience enough ranging for this effect to take place. This phenomenon changes the fluence which directly impacts the results of reconstruction techniques.

This effect can be mitigated by reducing the thickness of the aluminum filtering in the detector stack. For a standard configuration of 1500 μm CR-39, using 150 μm Al instead of 200 μm Al eliminates the non-uniformity. The increased energy of the D^3He protons on the CR-39 could result in a decreased detection efficiency. Accelerator experiments show that reducing the filtering does not impact the detection efficiency of the CR-39 for the reduced filtering thickness of 150 μm Al. The work shown here provides a way to mitigate the intrinsic profile non-uniformity for D^3He proton radiography. The existence of this non-uniformity also informs the design of proton radiography experiments. In particular, it could compromise the quality of radiographs when the detector is put too close to the backlighter. While not all CR-39 are the same thickness, the methods described here can be adapted for proton radiography filtering stack.

Future work is needed to explore how other mechanisms contribute to the total observed non-uniformity. Future work could also explore how proton radiography reconstructions are impacted by this non-uniformity. In addition, the realistic non-uniform thickness of the first piece of CR-39 in the detector stack could be considered.

ACKNOWLEDGMENTS

The authors would like to thank R. Frankel and E. Doeg for help with processing the CR-39 used herein. This work was supported in part by the U.S. Department of Energy NNSA MIT Center-of-Excellence under Contract DE-NA0003868 and by the National Laser Users Facility under Contract No. DE-NA0003938. This report was prepared as an account of work sponsored by an agency of the United States Government. Neither the United States Government nor any agency thereof, nor any of their employees, makes any warranty, express or implied, or assumes any legal liability or responsibility for the accuracy, completeness, or usefulness of any information, apparatus, product, or process disclosed, or represents that its use would not infringe privately owned rights. Reference herein to any specific commercial product, process, or service by trade name, trademark, manufacturer, or otherwise does not necessarily constitute or imply its endorsement, recommendation, or favoring by the United States Government or any agency thereof. The views and opinions of authors expressed herein do not necessarily state or reflect those of the United States Government or any agency thereof.

DATA AVAILABILITY

The data that support the findings of this study are available from the corresponding author upon reasonable request.

REFERENCES

[1]C. K. Li, F. H. Séguin, J. A. Frenje, and et al., Phys. Rev. Lett. **97** (2006).
[2]R. D. Petrasso, C. K. Li, F. H. Seguin, and et al., Phys. Rev. Lett. **103**, 085001 (2009).
[3]C. K. Li, F. H. Séguin, J. A. Frenje, and et al., Phys. Rev. Lett. **99**, 055001 (2007).
[4]J. A. Pearcy, M. J. Rosenberg, T. M. Johnson, and et al., Phys. Rev. Lett. **132** (2024).
[5]P. Tzeferacos, A. Rigby, A. F. A. Bott, and et al., Nat. Commun. **9** (2018).
[6]A. F. A. Bott, C. Graziani, P. Tzeferacos, and et al., J. Plasma Phys. **83** (2017).
[7]M. F. Kasim, L. Ceurvorst, N. Ratan, and et al., Phys. Rev. E. **95** (2017).
[8]J. A. Pearcy, G. D. Sutcliffe, T. M. Johnson, and et al., Appl. Opt. **63**, A98 (2024).
[9]M. Borghesi, A. Schiavi, D. H. Campbell, and et al., Plasma Phys. Control. Fusion **43**, A267 (2001).
[10]C. K. Li, F. H. Séguin, J. A. Frenje, and et al., Rev. Sci. Instrum. **77**, 10E725 (2006).
[11]D. B. Schaeffer, A. F. A. Bott, M. Borghesi, and et al., Rev. Mod. Phys. **95** (2023).
[12]M. J.-E. Manuel, A. B. Zylstra, H. G. Rinderknecht, and et al., Rev. Sci. Instrum. **83**, 063506 (2012).
[13]C. J. Waugh, M. J. Rosenberg, A. B. Zylstra, and et al., Rev. Sci. Instrum. **86**, 053506 (2015).
[14]T. R. Boehly, D. L. Brown, R. S. Craxton, and et al., Opt. Commun. **133**, 495 (1997).
[15]D. G. Hicks, C. K. Li, F. H. Séguin, and et al, Phys. Plasmas **7**, 5106 (2000).
[16]F. H. Séguin, J. A. Frenje, C. K. Li, and et al., Rev. Sci. Instrum. **74**, 975 (2003).
[17]A. B. Zylstra, J. A. Frenje, F. H. Séguin, and et al., Nucl. Instrum. Methods Phys. Res. A **681**, 84 (2012).
[18]T. M. Johnson, A. Birkel, H. E. Ramirez, and et al., Rev. Sci. Instrum. **92**, 043551 (2021).
[19]N. Sinenian, A. B. Zylstra, M. J.-E. Manuel, and et al., Appl. Phys. Lett. **101**, 114102 (2012).
[20]J. F. Ziegler, Nucl. Instrum. Methods Phys. Res. B **219-220**, 1027 (2004).
[21]R. Przybocki, M. G. Johnson, G. Sutcliffe, and et al., Rev. Sci. Instrum. **92**, 013504 (2021).
[22]B. Lahmann, M. Gatu Johnson, J. A. Frenje, and et al., Rev. Sci. Instrum. **91**, 053502 (2020).
[23]S. Agostinelli, J. Allison, K. Amako, and et al., Nucl. Instrum. Methods Phys. Res. A **506**, 250 (2003).
[24]J. Allison, K. Amako, J. Apostolakis, and et al., IEEE Trans. Nucl. Sci. **53**, 270 (2006).
[25]J. Allison, K. Amako, J. Apostolakis, and et al., Nucl. Instrum. Methods Phys. Res. A **835**, 186 (2016).
[26]N. Sinenian, M. J.-E. Manuel, A. B. Zylstra, and et al., Rev. Sci. Instrum. **83**, 043502 (2012).
[27]G. F. Knoll, *Radiation Detection and Measurement*, 4th ed. (John Wiley & Sons, Chichester, England, 2010).